



1 **Seasonal variation and influence factors of river water isotopes in the**
2 **East Asian monsoon region: A case study in Xiangjiang River basin**
3 **spanning 13 hydrological years**

4 Xiong Xiao¹, Xinping Zhang^{1,2*}, Zhuoyong Xiao¹, Zhiguo Rao¹, Xinguang He^{1,2},
5 Cicheng Zhang¹

6 ¹ *College of Geographic Science, Hunan Normal University, Changsha 410081, China*

7 ² *Key Laboratory of Geospatial Big Data Mining and Applications in Hunan Province,*
8 *Hunan Normal University, Changsha 410081, China*

9 **ABSTRACT:** Seasonal variation and influencing factors of water isotopes were
10 investigated in the Xiangjiang River basin, located in the East Asian monsoon region.
11 This involved comprehensive sampling of precipitation and river water, as well as
12 observing hydrometeorological factors spanning 13 hydrological years from January
13 2010 to December 2022. Key findings are as follows: River water $\delta^2\text{H}$ ($\delta^2\text{H}_R$)
14 exhibited significant seasonal variation, with the most positive and negative $\delta^2\text{H}_R$
15 occurring in the spring flood period and summer drought, respectively, and generally
16 aligned with those observed in precipitation. The correlations of the $\delta^2\text{H}_R$ with the
17 corresponding hydrometeorological factors were generally weak and the reasons can
18 be attributed to the seasonality of precipitation isotopes and mixing of various water
19 bodies within the basin, but the changes in the runoff (ΔR) and $\delta^2\text{H}_R$ ($\Delta\delta^2\text{H}_R$) between
20 two contiguous samplings showed significant responses to the corresponding
21 accumulated precipitation and evaporation. These results underscore the potential of
22 $\Delta\delta^2\text{H}_R$ as a variable that reflects the seasonal variations in local environments,
23 valuable for paleoclimate reconstruction. Prolonged rainless intervals with high
24 evaporation rates in 2013 and 2022, as well as significant precipitation events in

* Corresponding author. Tel.: +86-13308486020; E-mail address: zxp@hunnu.edu.cn



25 major flood periods in 2011 and 2017, notably had a significant impact on the $\delta^2\text{H}_R$
26 and runoff discharge. The most positive $\delta^2\text{H}_R$ values were primarily influenced by the
27 precipitation input with the most enriched isotopes in the spring flood period, while
28 the moderately isotope-depleted precipitation during limited basin wetness conditions
29 led to the most negative $\delta^2\text{H}_R$, thus caution is advised when interpreting extreme
30 isotopic signals in river water. The spatial correlation analysis between water isotopes
31 and hydrometeorological factors at the observing site and in the surrounding regions
32 supported the representation of the Changsha site in the Xiangjiang River basin.
33 Overall, these findings provide insights into the seasonal variation and influencing
34 factors of $\delta^2\text{H}_R$ in the study area, shedding light on the complex dynamics of river
35 water isotopes under different hydrometeorological conditions.

36 **Keywords:** Stable isotopes; River water; Precipitation input; Evaporation; Seasonal
37 variation.

38 1. Introduction

39 Stable isotopes of natural water possess exceptional sensitivity and serve as
40 remarkable recorders of environmental change, for instance, water bodies undergo
41 phase changes throughout the water cycle, resulting in stable isotope
42 fractionation—an occurrence where light or heavy stable isotope molecules are
43 distributed unequally between phases (Scholl et al., 2015; Xiao et al., 2022a).
44 Generally, during water phase changes, light isotope molecules tend to evaporate
45 more readily than heavy isotope molecules, while heavy isotope molecules
46 preferentially condense compared to their lighter counterparts (Craig, 1961;
47 Dansgaard, 1964). This isotope fractionation phenomenon contributes to variations in
48 stable isotopic compositions among different water bodies within the water cycle. As
49 a result, the relative ratios of stable isotopes in water serve as natural indicators of the



50 water cycle processes (Boral et al., 2019; Xiao et al., 2020; Wu et al., 2021) and find
51 extensive application in hydrometeorology and meteorological diagnosis (e.g.,
52 Aggarwal et al., 2016; Sinha et al., 2019; Zhiñá et al., 2022) and paleoclimate
53 reconstruction (e.g., Steinman et al., 2010; Jiménez-Iñiguez et al., 2022;
54 Emmanouilidis et al., 2022). For instance, the stable river water isotopes primarily
55 reflect the characteristics of precipitation, as precipitation input acts as the primary
56 water source (Sprenger et al., 2022; Wang et al., 2023). Moreover, due to varying
57 degrees of evaporation enrichment and mixing processes experienced by different
58 water bodies within a basin, the river water isotopes markedly differ from that of the
59 precipitation input and exhibit distinct seasonality (Jiang et al., 2021; Sun et al., 2021;
60 Das and Rai, 2022). This disparity forms the basis for employing stable isotope
61 techniques to investigate runoff generation processes in basins.

62 River water is commonly recognized as a natural integrator of basin hydrological
63 processes, offering insights into the effects of hydrometeorological factors like air
64 temperature, evaporation, precipitation input, and runoff discharge/water level (Yang
65 et al., 2020; von Freyberg et al., 2022). Extensive efforts have been made to
66 investigate the extent of variations in river water isotopes and examine the
67 relationship between stable isotopes in river water and specific environmental factors
68 (e.g., Yang et al., 2020; Das and Rai, 2022; Ren et al., 2023). However, in regions
69 where new water mixes thoroughly with old water, the river water isotopes exhibit
70 dampened signals, indicating that old water dominates the composition of stream
71 water and that the response of river water isotopes to hydrometeorological factors is
72 sluggish (Munoz-Villers and McDonnell, 2012; Streletskiy et al., 2015). Furthermore,
73 extreme precipitation and drought events have become more frequent under the
74 background of global climate changes, as evidenced in numerous regions worldwide



75 (Nkemelang et al., 2018; Cook et al., 2018; Grillakis, 2019; Marengo et al., 2020;
76 Cardoso et al., 2020). These events introduce additional complexities and intricate
77 seasonality in river stable isotopes on a basin scale, thus the identification of the
78 controlling factors that influence river water isotopes becomes challenging (Uchiyama
79 et al., 2017; Boutt et al., 2019; Saranya et al., 2020). The East Asian monsoon region,
80 characterized by complex water vapor sources, substantial seasonal and inter-annual
81 temperature and precipitation variations, as well as frequent floods and seasonal
82 droughts, further contributes to the hydrological complexity in this region (Huang et
83 al., 1998; Zhou et al., 2019; Wang et al., 2023). Hence, long-term observations of
84 river water isotopes and hydrometeorological factors, along with comprehensive
85 analyses of the influencing factors, are crucial to enhance our understanding of how
86 climate change impacts hydrological regimes in basins within the East Asian monsoon
87 region.

88 Long-term observations of water isotopes are crucial as they enable the capture
89 of extreme precipitation and drought events, facilitating an analysis of their influences
90 on river water isotopes, while also unveiling patterns of seasonal and inter-annual
91 variation (Rode et al., 2016; von Freyberg et al., 2022; Ren et al., 2023). However, the
92 long-term observations of river water isotopes with a high sampling frequency are
93 relatively challenging and rare due to logistical constraints (von Freyberg et al., 2017).
94 Therefore, in this study, the Xiangjiang River basin was selected as the study area to
95 investigate the seasonal variation and controlling factors of river water isotopes under
96 the influence of the monsoon. Extensive sampling of river water and precipitation,
97 along with the monitoring of hydrometeorological factors, was conducted over 13
98 complete hydrological years from January 2010 to December 2022. This study aims to
99 achieve the following objectives: (1) Identify the factors influencing the seasonality of

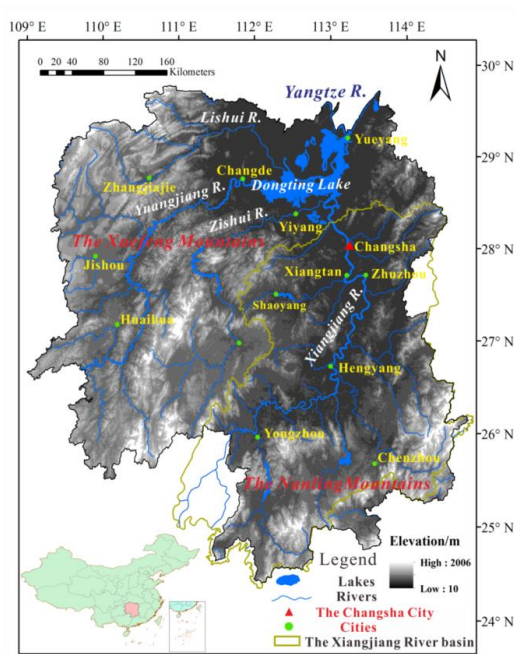


100 river water isotopes; (2) Assess the influences of extreme drought and precipitation
101 events on river water isotopes; (3) Interpret the environmental significance implied by
102 the seasonality of river water isotopes.

103 **2. Study site**

104 The study area was situated in a typical East Asian monsoon region,
105 characterized by distinct climatic variations throughout the four seasons. On average,
106 the annual precipitation and evaporation were 1147 mm and 902 mm, respectively
107 (Xiao et al., 2022b). Notably, there is a significant seasonal disparity in precipitation,
108 with an average of 152 rainy days each year. The period from early March to mid-July
109 experiences abundant precipitation due to the influence of the monsoon, whereas from
110 mid-July to September, drought conditions prevail as a result of the subtropical
111 high-pressure system. The average annual temperature in the region is 17.4 °C, and
112 the duration of the plant growing period spans approximately 330 days.

113 The Xiangjiang River basin, originating in the Guangxi Zhuang Autonomous
114 Region, encompasses a drainage area of 94,660 km². It stretches for 856 km
115 northward across Hunan Province, passing through cities like Hengyang, Xiangtan,
116 Zhuzhou, and Changsha (Fig. 1). The altitudinal range of the Xiangjiang River basin
117 varies from 1902 to 10 m, with higher elevations in the southern region characterized
118 by multiple terraces and valley landforms, while the northern part is relatively lower.
119 The middle and lower reaches of the Xiangjiang River basin are predominantly hilly
120 basins, surrounded by the Xuefeng Mountains and Nanling Mountains (Fig. 1).



121

122 Figure 1. Map showing the location of the Hunan Province, China and the Changsha
123 site.

124 3. Methods and materials

125 3.1 Water samples collection and analysis

126 From January 2010 to December 2022, the collection of river water and
127 precipitation samples was conducted.

128 River water sampling took place 929 times at the center of Orange Island, with a
129 regular sampling interval of five days. Specifically, samples were obtained on the 1st,
130 6th, 11th, 16th, 21st, and 26th days of each month. The sampling depth of river water
131 was relatively deep to avoid the influences of human activity; moreover, this
132 operation can avoid the evaporation fractionation of surface water during the sampling
133 and ensure adequate mixes of the river water.

134 At the College of Geographic Science, Hunan Normal University, Changsha (Fig.



135 1, 112°56'28" E, 28°11'30" N), the sampling of precipitation and the measurements of
136 precipitation amount were conducted at the altitude of 55 m, adjacent to the Yuelu
137 Mountains, throughout the sampling period of this study (2010–2022). For
138 precipitation sampling, a siphon rain gauge was repurposed as a collector, consisting
139 of a 6-cm diameter funnel connected to a glass bottle via a plastic pipe. Both rainfall
140 and snowfall were collected and measured at 8:00 and 20:00 local time on the
141 precipitation day, and the volume-weighted value of the two samplings was used to
142 represent the precipitation isotopic values of the day, while the precipitation amount
143 of the day was calculated by the sum of the two samplings. Snowfall samples were
144 carefully packed in sealed plastic bags, which were later melted at room temperature.
145 A total of 1668 precipitation isotopic values were obtained over 1668 precipitation
146 days. Furthermore, considering that the sampling interval for river water was set at
147 five days, and previous studies have indicated that it may take 3-5 days for
148 precipitation (new water) to significantly contribute to river water (Yao et al., 2016;
149 Xiao et al., 2022a), the precipitation isotopes were volume-weighted in the 5-day
150 interval within this study.

151 To ensure proper preservation, both the river water and precipitation samples
152 were transferred to clean, sealed, polyethylene bottles (30 ml) and stored in a
153 refrigerator at 0 °C. However, few precipitation and river water samples were lost,
154 resulting in some missing data. Further details regarding the sample collection
155 procedures can be found in Xiao et al. (2022a). The isotopic composition of the
156 samples was determined using the off-axis integrated cavity output spectroscopy
157 method, specifically conducted with equipment from Los Gatos Research in the USA.
158 The stable isotopic composition in the water samples is reported in ‰ (per mil). For a
159 comprehensive description of the analytical procedures employed, please refer to the



160 detailed account provided by Xiao et al. (2022b).

161 **3.2 Hydrometeorological observations**

162 The daily air temperature and evaporation data used in this study were obtained
163 from the National Meteorological Reference Station in Changsha (station code:
164 57687), specifically utilizing the large evaporator model E-601B. It is worth noting
165 that the evaporation recorded by the E-601B evaporator closely approximates the
166 actual evaporation experienced in small water bodies such as lakes and rivers. As such,
167 it reliably represents the quantity and temporal variations of evaporation within the
168 study area (Hua et al., 2019).

169 Daily runoff discharge data were obtained from the Xiangtan hydrological station
170 (station code: 61102000). Following the national standard “Code for liquid flow
171 measurement in open channels” (GB 50179-93, 1993) issued by the Ministry of Water
172 Resources of the People’s Republic of China, the daily discharge values are calculated
173 by applying the weighted average of intraday instantaneous discharge. This
174 calculation is based on water level observations and a specific stage-discharge curve.
175 As per the guidelines outlined in GB 50179-93, the relative errors in instantaneous
176 discharge measurements range from 2% for high water levels, 5% for normal water
177 levels, and 9% for low water levels. On average, the estimated annual discharge falls
178 within 5% of the actual value. To facilitate the comparison of runoff discharge with
179 precipitation and evaporation, the daily runoff discharge data (in m^3/d) are normalized
180 by dividing them by the basin area (in m^2) of the measuring cross-section.
181 Consequently, the runoff depth (in m/d or mm/d) and runoff discharge data (in m^3/d)
182 are computed and utilized in the subsequent analysis.

183 **4. Results**

184 **4.1 Stable isotopic characteristics of precipitation and river water**



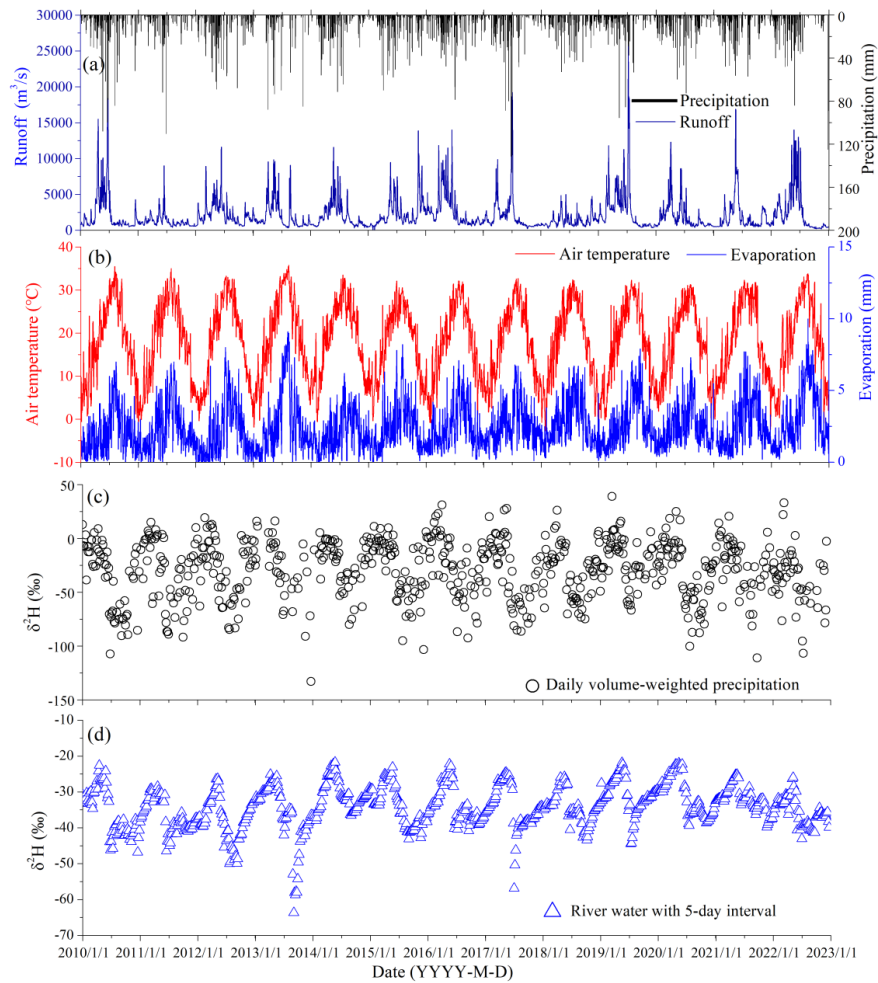
185 Table 1 presents the monthly average values of air temperature ($^{\circ}\text{C}$), precipitation
186 (mm), evaporation (mm), and runoff discharge (10^8 m^3), and the results illustrate the
187 uneven distribution of these factors throughout the year. Based on the monthly
188 patterns of these hydrometeorological factors (Table 1) and the previous findings (Qin
189 et al., 2006; Yao et al., 2016), four distinct runoff periods have been identified: the
190 rainless period, spring flood period, major flood period, and summer drought period.
191 The rainless period spans from October to the following February, characterized by
192 low air temperature, minimal precipitation, evaporation, and runoff discharge. In this
193 period, the runoff discharge exhibits slight fluctuations except for isolated peaks
194 resulting from major rainfall events; The spring flood period, occurring in March and
195 April, marks an increase in runoff discharge, this can be attributed to relatively higher
196 precipitation amounts, as well as moderate air temperature and evaporation in spring;
197 The major flood period, extending from May to mid-July, exhibits a rapid surge in
198 runoff discharge, often reaching peak values due to intensive precipitation events; The
199 summer drought period, which spans from mid-July to September, while a significant
200 decrease in runoff discharge is always observed. This decline can be attributed to high
201 air temperature leading to increased evaporation in this period. Additionally, the
202 scarcity of precipitation events and relatively low precipitation amounts contribute to
203 the reduced runoff discharge in this period. Overall, the analysis highlights the
204 seasonal variations in air temperature, precipitation, evaporation, and runoff discharge,
205 leading to distinct runoff periods throughout the year.
206



207 Table 1. Monthly average air temperature (°C), precipitation (mm), evaporation
208 (mm), and runoff discharge (10^8 m^3)

| Month | Air Temperature | Precipitation | Evaporation | Runoff discharge |
|-------|-----------------|---------------|-------------|---------------------------|
| | °C | mm | mm | $\times 10^8 \text{ m}^3$ |
| Jan. | 5.6 | 68.9 | 33.0 | 35.5 |
| Feb. | 7.6 | 82.3 | 33.8 | 35.7 |
| March | 12.7 | 150.0 | 46.4 | 65.1 |
| April | 17.8 | 145.6 | 60.8 | 85.5 |
| May | 22.2 | 230.6 | 71.9 | 111.7 |
| June | 26.1 | 212.3 | 80.6 | 115.0 |
| July | 29.4 | 156.7 | 132.4 | 71.9 |
| Aug. | 28.9 | 87.6 | 141.7 | 36.0 |
| Sep. | 24.8 | 84.2 | 105.3 | 26.8 |
| Oct. | 18.7 | 61.2 | 83.9 | 22.0 |
| Nov. | 13.6 | 82.7 | 53.9 | 38.1 |
| Dec. | 7.5 | 54.6 | 47.5 | 31.8 |

209 Because the $\delta^2\text{H}$ and $\delta^{18}\text{O}$ of river water and precipitation samples were very
210 similar, for the aims to keep with the previous analysis of the Xiangjiang River water
211 isotopes (i.e. Xiao et al., 2022a) the temporal variations of $\delta^2\text{H}$ values are mainly
212 discussed in this paper. From 2010 to 2022, the 5-day volume-weighted precipitation
213 $\delta^2\text{H}$ ($\delta^2\text{H}_p$) exhibited large seasonality throughout the year, as depicted in Fig. 2 and
214 Fig. 3. Notably, the 5-day volume-weighted $\delta^2\text{H}_p$ ranged from -133.0‰ to 39.1‰ ,
215 with a standard deviation of 27.6‰ . The 5-day volume-weighted $\delta^2\text{H}_p$ showed the
216 maximum values in March, while the minimum values occurred in September (Fig.
217 2c). Furthermore, the 5-day volume-weighted $\delta^2\text{H}_p$ followed the following order:
218 spring flood period > rainless period > major flood period > summer drought period
219 (Fig. 3b). The seasonal variations in the precipitation isotopes primarily result from
220 different vapor sources, upstream effects, circulation patterns, and local
221 meteorological factors in different seasons (Zhou et al., 2019; Xiao et al., 2023). The
222 $\delta^2\text{H}$ values of river water ($\delta^2\text{H}_R$) ranged from -63.7‰ to -21.7‰ , with a standard
223 deviation of 6.1‰ (Figs. 2 and 3).

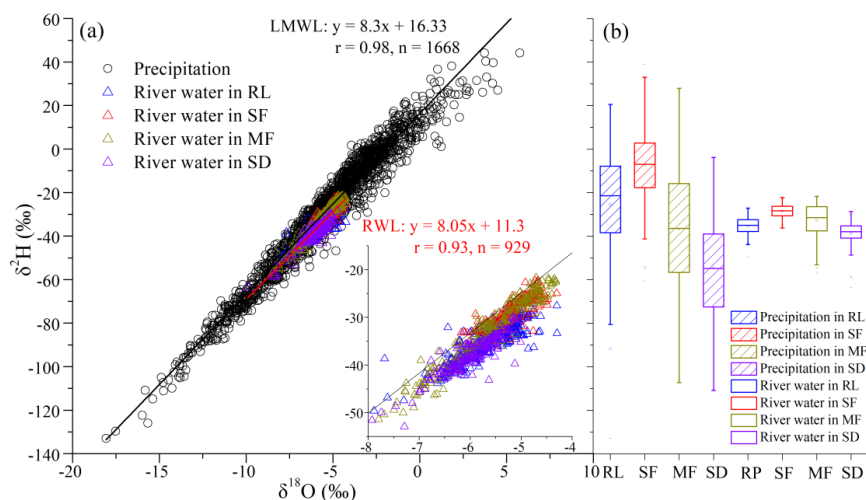


224

225 Figure 2. Temporal variation of the daily runoff discharge and precipitation (a), daily

226 air temperature and evaporation (b), daily volume-weighted precipitation $\delta^2\text{H}$ (c), and

227 river water $\delta^2\text{H}$ with 5-day interval (d).



228

229 Figure 3. Stable isotope composition ($\delta^2\text{H}$ and $\delta^{18}\text{O}$) of daily volume-weighted
230 precipitation and river water samples (a) and box plots of precipitation and river water
231 $\delta^2\text{H}$ (b) in different periods (rainless period, spring flood period, major flood period,
232 and summer drought period). LMWL (black solid line) and RWL (red solid line)
233 represent the local meteoric water line and river water line based on all the
234 precipitation and river water isotopic data from January 2010 to December 2022,
235 respectively. The letters (RL, SF, MF, and SD) in the x-axis represent the rainless
236 period, spring flood period, major flood period, and summer drought period,
237 respectively.

238 The magnitude of $\delta^2\text{H}_R$ was ranked as follows: spring flood period, major flood
239 period, rainless period, and summer drought period (Fig. 3b). The most depleted and
240 enriched isotopic values in river water in the sampling period occurred on September
241 1, 2013, and May 21, 2014, respectively (Fig. 2). The seasonal variations in river
242 water isotopes generally aligned with those observed in precipitation, indicating that
243 river water directly derives from the precipitation input and is influenced by its
244 isotopic composition. Moreover, the local meteoric water line (LMWL) and river



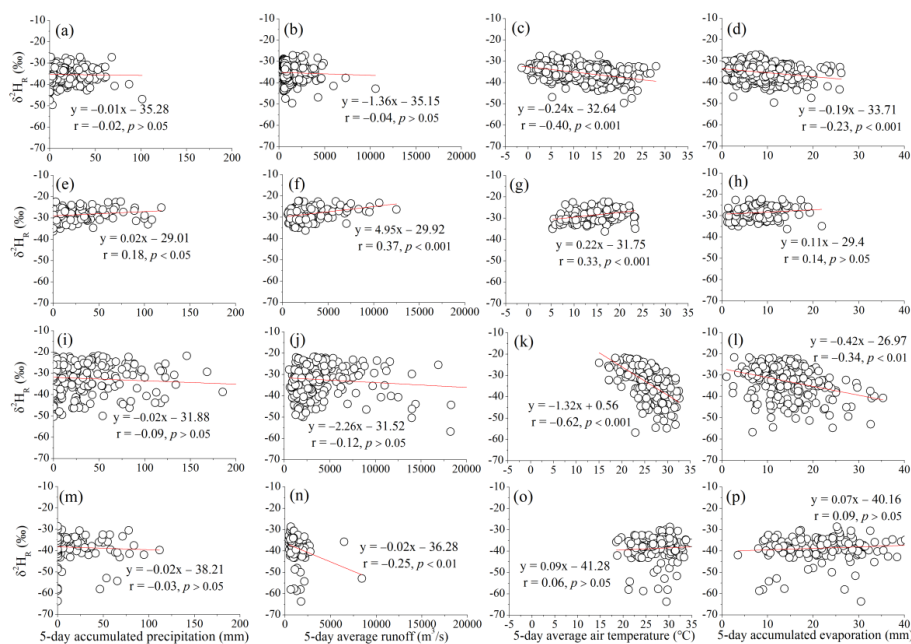
245 water line (RWL) have a relatively close slope of 8.3 and 8.05, respectively (Fig. 3a).
246 However, the $\delta^2\text{H}_R$ exhibited a relatively smaller range of variation and more
247 attenuated temporal pattern compared to the $\delta^2\text{H}_P$. This is likely due to the processes
248 that precipitation undergoes before recharging river water, such as evaporation and
249 mixing with older waters, which significantly reduce the variability in $\delta^2\text{H}_R$ (Xiao et
250 al., 2022a).

251 **4.2 Relationship between river water isotopes and various** 252 **hydrometeorological factors**

253 The relationships between the $\delta^2\text{H}_R$ and the corresponding 5-day accumulated
254 precipitation and evaporation and average runoff discharge and air temperature in
255 different periods are illustrated in Fig. 4. Based on the relationship between the 5-day
256 volume-weighted $\delta^2\text{H}_P$ and the corresponding accumulated precipitation in different
257 runoff periods (Fig. S1; left panel), it is evident that an “amount effect” is observed in
258 the precipitation isotopes across various runoff periods. Specifically, the increased
259 precipitation amounts consistently result in more isotope-depleted precipitation.
260 Furthermore, the $\delta^2\text{H}_R$ exhibits a positive correlation versus the corresponding 5-day
261 volume-weighted $\delta^2\text{H}_P$, with a correlation coefficient of 0.55 and $p < 0.001$ (Fig. S2).
262 This suggests that precipitation input is the primary factor influencing $\delta^2\text{H}_R$. However,
263 as shown in Fig. 4, the $\delta^2\text{H}_R$ exhibited relatively weak correlations with the
264 corresponding 5-day accumulated precipitations in the rainless period, major flood
265 period, and summer drought period, as indicated by low correlation coefficient values
266 and $p > 0.05$ (Fig. 4a, 4i, 4m). Although a positive correlation between $\delta^2\text{H}_R$ and the
267 corresponding 5-day accumulated precipitations in the spring flood period, their
268 correlation coefficients were not exceptionally high (Fig. 4e). The weak correlation
269 between the $\delta^2\text{H}_R$ and precipitation amount or runoff discharge can be attributed to the



270 expansive area and water reserves in the Xiangjiang River basin—that is, after
 271 precipitation falls in the basin and the new input precipitation within 5 days may
 272 influence the $\delta^2\text{H}_R$ to some extent, however, it tends to mix with old waters, such as
 273 groundwater, soil water, and river water consists of a high proportion of older water
 274 components, thereby attenuating the impact of precipitation input and predominantly
 275 shape the river water isotopes.



276
 277 Figure 4. Relationships between the river water $\delta^2\text{H}$ and the corresponding 5-day
 278 accumulated precipitation (the first column), 5-day average runoff discharge (the
 279 second column), 5-day average air temperature (the third column), and 5-day
 280 accumulated evaporation (the fourth column) in different periods, and the first row (a,
 281 b, c, and d), the second row (e, f, g, and h), the third row (i, j, k, and l), and the fourth
 282 row (m, n, o, and p) represent the rainless period, spring flood period, major flood
 283 period, and summer drought period, respectively.

284 The $\delta^2\text{H}_R$ exhibits a consistent relationship with the corresponding 5-day average



285 air temperature and accumulated evaporation within each respective runoff period.
286 However, positive or negative correlations may be observed in these relationships
287 across the four runoff periods. Specifically, in the spring flood period and summer
288 drought period, the $\delta^2\text{H}_R$ demonstrates either a significant ($p < 0.001$) or
289 non-significant ($p > 0.05$) positive correlation with the corresponding 5-day average
290 air temperature and accumulated evaporation (Fig. 4g-h and 4o-p). Conversely, in the
291 rainless period and major flood period, a significant ($p < 0.001$ or $p < 0.01$) negative
292 correlation is observed (Fig. 4c-d and 4k-i). The negative relationship between the
293 $\delta^2\text{H}_R$ and the corresponding 5-day average air temperature or accumulated
294 evaporation may seem counterintuitive, as river water isotopes typically become
295 enriched with increasing air temperature and progressing evaporation (Gibson et al.,
296 2016; Jiang et al., 2021). This discrepancy can be explained by considering the
297 seasonality of the relationship between precipitation isotopes and air temperature in
298 different runoff periods (Fig. S1; right panel). For instance, the 5-day
299 volume-weighted $\delta^2\text{H}_P$ gradually decreases as the corresponding average air
300 temperature increases in the major flood period, while increasing as the corresponding
301 average air temperature decreases in the rainless period (Fig. 2 and 3). This would
302 lead to the negative relationship between the 5-day volume-weighted $\delta^2\text{H}_P$ and the
303 corresponding average air temperature in the rainless period and major flood period
304 (Fig. S1b and S1f), subsequently resulting in the negative relationship between the
305 $\delta^2\text{H}_R$ and the corresponding 5-day average air temperature in these two periods (Fig.
306 4c-d and 4k-i). Moreover, as there is strong consistency between evaporation and air
307 temperature (Allen et al., 2005), this alignment causes evaporation to also exhibit a
308 negative correlation with $\delta^2\text{H}_R$ in these two periods (Fig. 4). Therefore, in the major
309 flood period and rainless period, the influences of air temperature and evaporation on



310 river water isotopes are somewhat masked by the seasonality of precipitation isotopes.

311 In the spring flood period and summer drought period, the river water isotopes
312 exhibited an enrichment trend with the increasing of the corresponding average air
313 temperature and accumulated evaporation (Fig. 4g-h and 4o-p). However, these
314 relationships may be somewhat misleading due to the positive correlation observed
315 between the 5-day volume-weighted $\delta^2\text{H}_p$ and the corresponding average air
316 temperature in the spring flood period ($p < 0.05$) and summer drought period ($p >$
317 0.05) (Fig. S1d and S1h). This suggests that the positive correlation between river
318 water isotopes and air temperature or evaporation may also be influenced by the
319 seasonality of precipitation isotopes. Moreover, in the spring flood period, the
320 increases in precipitation amount and runoff discharge lead to more isotope-enriched
321 river water, as indicated in Fig. 4e and 4f. This phenomenon can be attributed to the
322 most enriched precipitation isotopes occurring in the spring flood period (Fig. 2c and
323 3b), as the precipitation amount and runoff discharge gradually increase in this period
324 (Fig. 2a), it contributes to the positive relationship observed between the $\delta^2\text{H}_R$ and the
325 corresponding accumulated precipitation or average runoff discharge. Consequently,
326 based on the findings of this section, when interpreting the relationships between the
327 river water isotopes and hydrometeorological factors, it is important to consider the
328 uncertainty arising from the seasonality of precipitation isotopes.

329 **4.3 Relationship between the changes in river water isotope and the** 330 **precipitation and evaporation**

331 As shown in Fig. 4, the relationship between the $\delta^2\text{H}_R$ and various factors may
332 not be significant or may contradict common sense—that is, precipitation input and
333 evaporation are likely the major driving factors that change the isotopic compositions
334 of river water. For instance, the river water isotopes tend to be more depleted and the

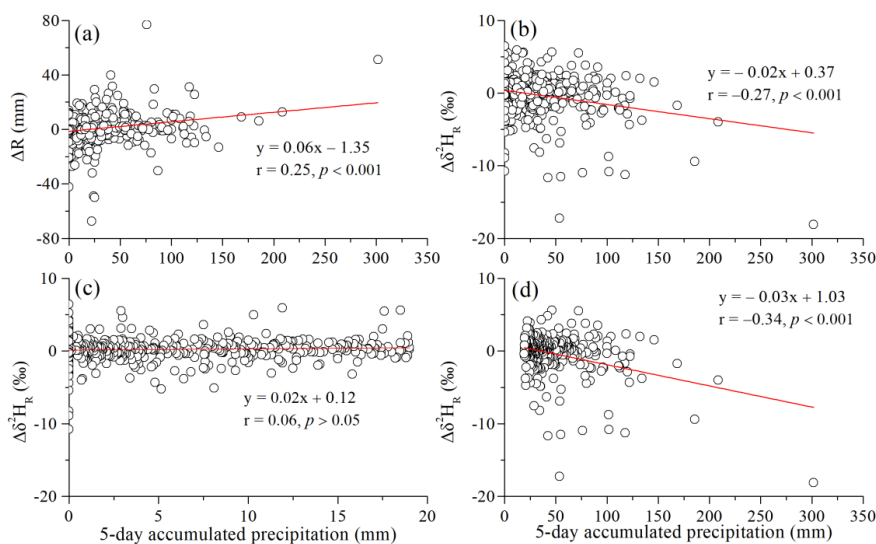


335 slope of RWL tends to be high in heavy precipitation events, while the river water
336 generally exhibits gradual enriched stable isotopes and lower evaporation line slope
337 on rainless days with high air temperature and evaporation (Gibson et al., 2016; Yang
338 et al., 2020; Jiang et al., 2021). Therefore, under the river water sample collection at a
339 5-day interval, it is essential to analyze the influences of the individual
340 hydrometeorological factors on the changes in the $\delta^2\text{H}_R$ between two contiguous
341 samplings ($\Delta\delta^2\text{H}_R$), which was calculated by the $\delta^2\text{H}_R$ differences between the $\delta^2\text{H}_R$ of
342 the following and preceding samplings (i.e. $\Delta\delta^2\text{H}_R = \delta^2\text{H}_R(t) - \delta^2\text{H}_R(t-1)$).

343 The 5-day runoff depth changes (i.e. $\Delta R = R(t) - R(t-1)$) and $\Delta\delta^2\text{H}_R$ exhibited
344 significant increases and decreases, respectively ($p < 0.001$), in response to the 5-day
345 accumulated precipitation (Fig. 5a and 5b). These findings indicate that precipitation
346 input is the primary factor influencing the variations in runoff discharge and river
347 water isotopes. Furthermore, based on the intersections between the linear fitting line
348 and the x-axis, the thresholds for precipitation amounts influencing the $\Delta\delta^2\text{H}_R$ and ΔR
349 at 5-day interval were determined to be 19.0 mm and 19.4 mm, respectively. This
350 suggests that heavier precipitation events are more likely to alter the river water
351 isotopes. The weak correlation ($p > 0.05$) between the $\Delta\delta^2\text{H}_R$ and corresponding 5-day
352 accumulated precipitation below the threshold value of 19.0 mm supports this
353 observation (Fig. 5c). Conversely when the 5-day accumulated precipitation exceeded
354 19.0 mm, a significant ($p < 0.001$) negative correlation was observed between the
355 $\Delta\delta^2\text{H}_R$ and the corresponding 5-day accumulated precipitation (Fig. 5d). In other
356 words, greater 5-day accumulated precipitation led to more negative $\delta^2\text{H}$ values in the
357 subsequent river water sample, with a correlation coefficient of -0.34 and $p < 0.001$.
358 Therefore, it can be concluded that the variation in river water isotopes reflects the
359 isotopic signal of the input precipitation, and the isotopic composition of river water



360 exhibits a significant “amount effect” by the precipitation input.



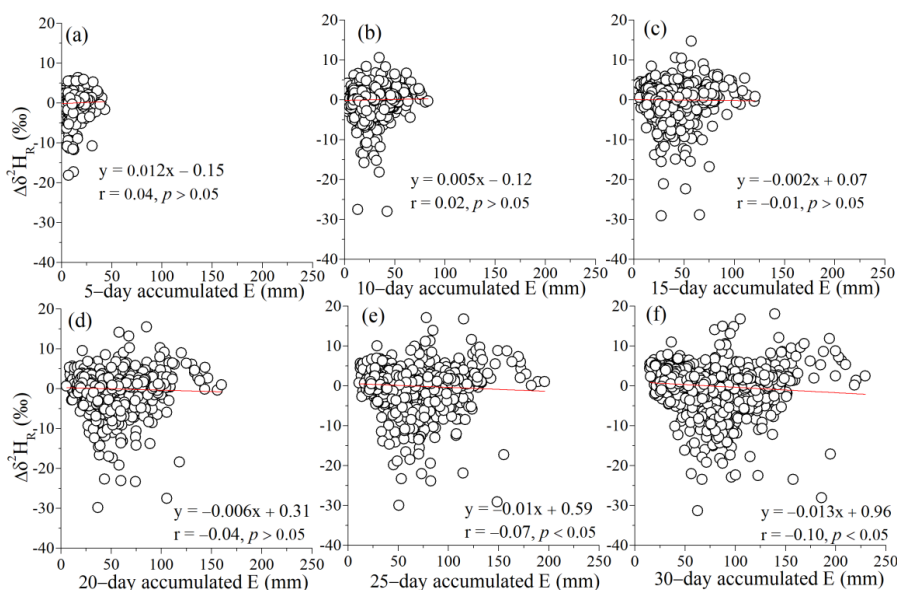
361

362 Figure 5. Relationship between the 5-day accumulated precipitation and the changes
363 in 5-day runoff discharge (ΔR) (a) and river water δ^2H ($\Delta\delta^2H_R$) (b), and the
364 relationship between the $\Delta\delta^2H_R$ and the corresponding 5-day accumulated
365 precipitation < 19.0 mm and > 19.0 mm were shown in subplot (c) and (d),
366 respectively.

367 Because of the confluence processes of the river water from upstream to
368 downstream and the mixing processes between the new and old waters, river water
369 may consist of a certain proportion of old water with a relatively long residence time
370 (Xiao et al., 2022a), thus we analysis the relationship between the river water isotopes
371 and the hydrometeorological factors at longer time interval. The relationships between
372 the $\Delta\delta^2H_R$ and corresponding accumulated evaporation at various time intervals (5-,
373 10-, 15-, 20-, 25-, and 30-day) were shown in Fig. 6. As there is strong consistency
374 between evaporation and air temperature (Allen et al., 2005), the relationship between
375 the $\Delta\delta^2H_R$ and air temperature was not analyzed in this paper. The results revealed a
376 weak and statistically non-significant correlation between the $\Delta\delta^2H_R$ and



377 corresponding accumulated evaporation at the 5-, 10-, 15-, and 20-day intervals (Fig.
378 6a-d). However, a significant ($p < 0.05$) negative correlation with relatively low
379 correlation coefficients was observed at the 25- and 30-day intervals (Fig. 6e and 6f).
380 The negative relationship between the $\Delta\delta^2H_R$ and the corresponding accumulated
381 evaporation (Fig. 6c-f) also contradicts the common sense that the river water
382 generally becomes more enriched under the influences of evaporation. This may be
383 due to the negative relationship between the δ^2H_P/δ^2H_R and the corresponding average
384 air temperature/accumulated evaporation in the rainless period and major flood period
385 (Fig. 2 and 3) as discussed earlier, besides, the effect of dilution precipitation input on
386 river water isotopes (Fig. 5 and S1) and the relatively low air temperature and high
387 relative humidity in the heavy precipitation events may be greater than the enrichment
388 effect of evaporation (e.g., similar as the effect demonstrated in Xiao et al., 2022b).



389

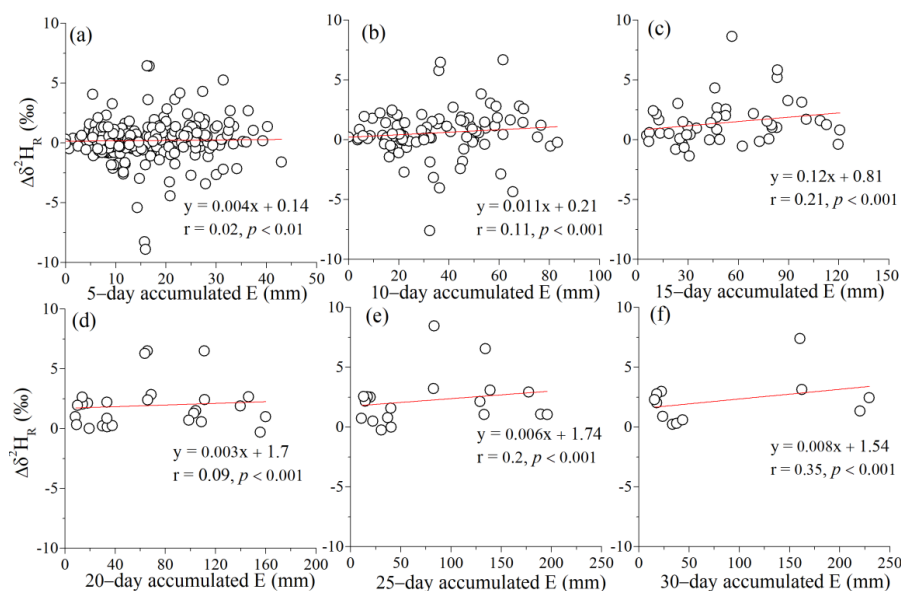
390 Figure 6. Relationship between the changes in river water δ^2H ($\Delta\delta^2H_R$) and the

391 corresponding accumulated evaporation (E) at 5-day (a), 10-day (b), 15-day (c),

392 20-day (d), 25-day (e), and 30-day (f) time intervals.



393 To highlight the influences of evaporation on the river water isotopes and
394 eliminate the influence of precipitation input, we analyzed the relationship between
395 the $\Delta\delta^2\text{H}_R$ and the corresponding accumulated evaporation at different intervals (5-,
396 10-, 15-, 20-, 25-, and 30-day) without precipitation input (Fig. 7). The findings
397 revealed a significant ($p < 0.01$ or $p < 0.001$) positive correlation between these
398 variables at different time intervals. In other words, as the accumulated evaporation
399 increased, the $\Delta\delta^2\text{H}_R$ also increased, with the correlation coefficient generally
400 increasing with longer rainless intervals. Notably, the influence of greater evaporation
401 on the $\Delta\delta^2\text{H}_R$ was particularly pronounced at the 30-day interval, exhibiting a high
402 correlation coefficient of 0.35 and a p value less than 0.001, while these intervals
403 occurred exclusively in 2013 and 2022, which were characterized as very dry years
404 with high evaporation and multiple 30-day intervals devoid of precipitation (Fig. 2
405 and S3).



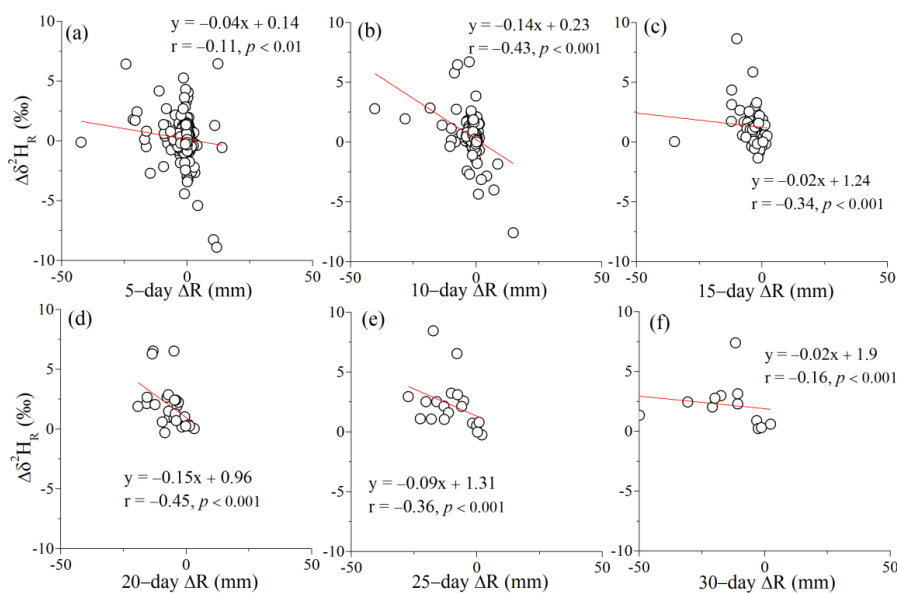
406

407 Figure 7. Relationship between the changes in river water $\delta^2\text{H}$ ($\Delta\delta^2\text{H}_R$) and the
408 corresponding accumulated evaporation (E) at 5- (a), 10- (b), 15- (c), 20- (d), 25- (e),



409 and 30- (f) rainless time intervals.

410 The decrease in runoff discharge or water level in the basin can be attributed to
411 evaporation within the basin, as evaporation increases the outflow component in the
412 river water balance, leading to a reduction in the amount of water flowing out of the
413 basin. Additionally, as runoff discharge can increase due to precipitation input, we
414 examined the relationship between the $\Delta\delta^2H_R$ and the corresponding changes in the
415 runoff (ΔR) at different intervals (5-, 10-, 15-, 20-, 25-, and 30-day) without
416 precipitation input (Fig. 8). The results indicated a negative correlation between the
417 $\Delta\delta^2H_R$ and the corresponding ΔR at the 10-, 15-, 20-, and 25-day intervals,
418 demonstrating relatively high correlation coefficients around -0.4 and p values less
419 than 0.001 . Considering the higher correlation coefficients observed between the
420 $\Delta\delta^2H_R$ and the corresponding ΔR (Fig. 8) compared to those between the $\Delta\delta^2H_R$ and
421 the corresponding accumulated evaporation (Fig. 7), it can be inferred that the ΔR
422 serves as a suitable proxy to represent the effects of evaporation on river water
423 isotopes. However, the correlation between the $\Delta\delta^2H_R$ and the corresponding ΔR was
424 relatively weak at the 5-day intervals, with correlation coefficients of -0.11 (Fig. 8a),
425 thus could be attributed to the short time interval and the limited impact of
426 accumulated evaporation.



427

428 Figure 8. Relationship between the changes in river water $\delta^2\text{H}$ ($\Delta\delta^2\text{H}_R$) and runoff
429 depth (ΔR) at 5- (a), 10- (b), 15- (c), 20- (d), 25- (e), and 30- (f) rainless time
430 intervals.

431 4.4 Influences of extreme drought and precipitation events on the 432 river water isotopes

433 Analysis of the annual accumulated evaporation, average air temperature,
434 accumulated precipitation, and average runoff discharge in the major flood period and
435 summer drought period reveals that 2013 and 2022 experienced severe summer
436 drought conditions (Fig. S3). These periods were characterized by exceptionally high
437 temperatures and evaporation and low precipitation levels compared to the 13-year
438 observations, particularly in 2022. The summer drought period of 2022 recorded only
439 16.3 mm of precipitation, the lowest among the 13-year observations and significantly
440 lower than the highest precipitation recorded in the summer drought period of 2010
441 (i.e. 300.5 mm). Accumulated evaporation and average air temperature in the summer

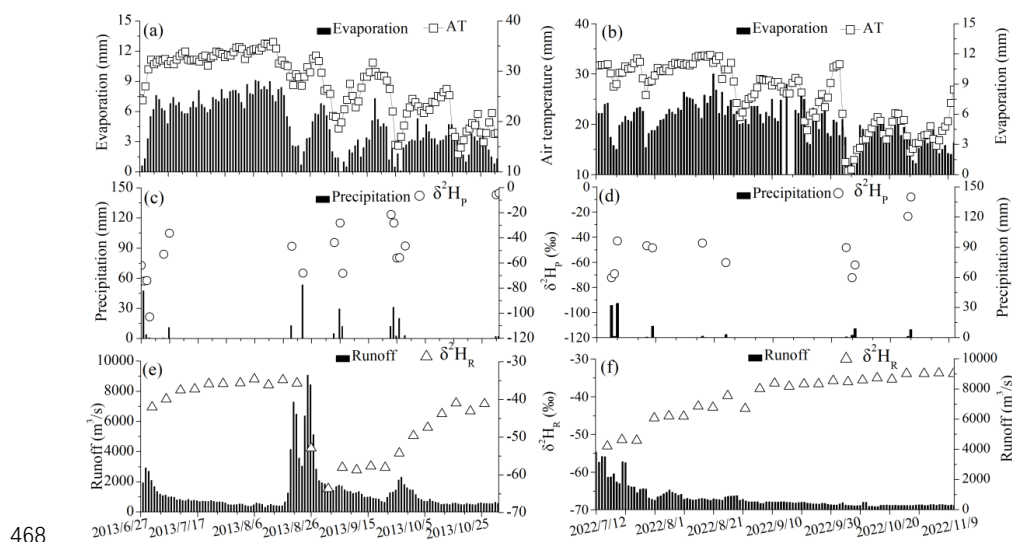


442 drought period of 2022 reached 385.1 mm and 28.8 °C, second only to the 393.7 mm
443 and 29.8 °C recorded in the summer drought period of 2013 (Fig. 3). Furthermore, the
444 extreme drought events in 2013 and 2022 have been extensively reported, indicating
445 widespread meteorological, hydrological, and soil droughts that pose a significant
446 threat to water resources for domestic, agricultural, ecological, and human needs (Ma
447 et al., 2022; Bonaldo et al., 2023). Therefore, this section primarily focuses on these
448 two extreme drought processes in 2013 and 2022.

449 As depicted in Fig. 9, the period from late June to mid-August 2013 witnessed
450 rare precipitation, high evaporation rates, and elevated air temperatures. Consequently,
451 the runoff discharge gradually decreased from 2699 m³/s on June 30 to 415 m³/s on
452 August 16. Simultaneously, the $\delta^2\text{H}_R$ progressively increased from -42.0‰ to -34.8‰
453 (Fig. 9e). Similarly, from mid-July to early November 2022, only 72.6 mm of
454 precipitation was recorded, resulting in a gradual decline in runoff discharge until
455 early September. In this process, the $\delta^2\text{H}_R$ increased from -53.1‰ on July 16 to
456 -37.9‰ on September 6 (Fig. 9f). Subsequently, the Xiangjiang River maintained low
457 runoff discharge and raised $\delta^2\text{H}_R$ levels until the end of December, and the $\delta^2\text{H}_R$
458 increased by up to 20.2‰ from -53.1‰ on July 16 to -32.9‰ on November 26, 2022
459 (Fig. 9f). These findings align with the results obtained in the previous section,
460 indicating that decreases in runoff discharge and higher evaporation rates in long
461 rainless days contribute to the gradual enrichment of river water isotopes. However, it
462 is noteworthy that the $\delta^2\text{H}_R$ range (-63.7‰ to -21.7‰) mentioned earlier includes the
463 most positive $\delta^2\text{H}_R$ values influenced by the extreme drought events in 2013 and 2022
464 (Fig. 2d), while the most isotope-enriched river water occurred on May 21, 2014 (Fig.
465 2d) and most isotope-enriched precipitation occurred in the spring flood period (Fig.
466 3b), this indicates that the input of relatively enriched spring precipitation isotopes



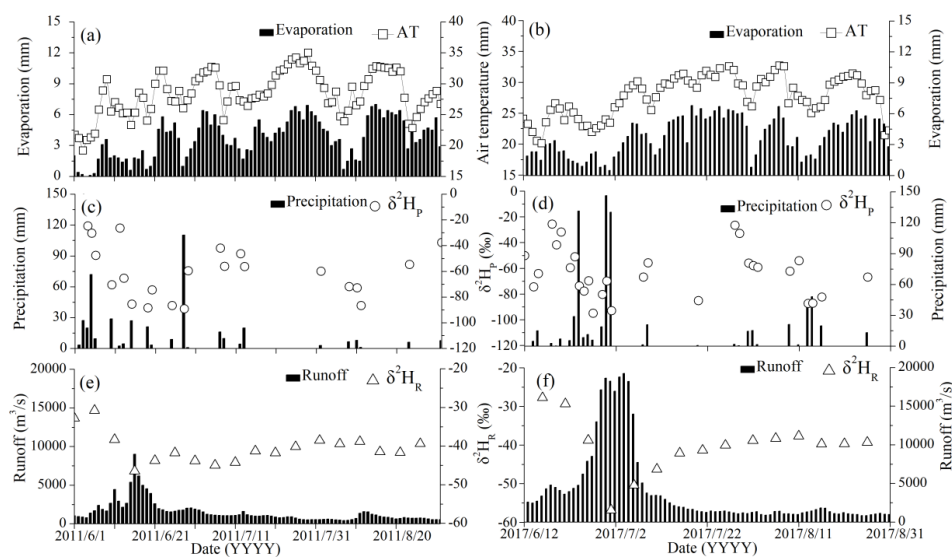
467 plays a crucial role in controlling the isotopic enrichment of river water.



468

469 Figure 9. Temporal variations of evaporation and air temperature (a, b), daily
470 precipitation amount and precipitation δ^2H (δ^2H_p) (c, d), and runoff discharge and
471 river water δ^2H (δ^2H_R) (e, f) in the extreme drought processes in 2013 (left panel) and
472 2017 (right panel).

473 By examining the 13-year observations and ranking the 5-day accumulated
474 precipitation, it was found that the maximum accumulated precipitation, totaling
475 301.6 mm, occurred from June 27 to July 1, 2017 (Fig. 2). Notably, on June 30 and
476 July 1, 2017, daily precipitation reached 146.4 mm and 130.3 mm, respectively.
477 Additionally, between June 21 and June 26, 2017, the precipitation amount reached
478 185.5 mm. Another significant precipitation event took place in June 2011, when the
479 total precipitation for the month reached 340.3 mm, with a single-day rainfall of 110.4
480 mm on June 28. To analyze the impact of extreme precipitation on river water
481 isotopes in the major flood period, the temperature, evaporation, precipitation, runoff
482 discharge, δ^2H_p , and δ^2H_R in these two extreme precipitation processes are presented
483 in Fig. 10.



484

485

486

487

488

Figure 10. Temporal variations of the evaporation and air temperature (a, b), precipitation amount and precipitation δ^2H (c, d), and runoff discharge and river water δ^2H (e, f) in the extreme precipitation processes and the following summer drought period in 2011 (left panel) and 2017 (right panel).

489

490

491

492

493

494

495

496

497

498

499

500

In the heavy precipitation period from June 5 to June 16, 2011, the runoff discharge increased from 1410 m³/s to 9010 m³/s, while the δ^2H_R decreased from -30.8‰ to -46.5‰ (Fig. 10e). Similarly, from June 21 to July 1, 2017, the runoff discharge and river water isotopes exhibited significant fluctuations and depletion under the influence of precipitation input (Fig. 10f). For instance, the runoff discharge increased from 3961 m³/s to 18237 m³/s, while the δ^2H_R decreased from -29.3‰ to -56.8‰, which represents the third lowest δ^2H_R value among the 13-year observations. In both extreme precipitation processes, the precipitation isotopes were relatively depleted (Fig. 10c and 10d). Specifically, the volume-weighted δ^2H_P was -50.9‰ from June 5 to June 16, 2011, and the value was -76.7‰ from June 21 to July 1, 2017. This indicates that the input of extreme precipitation leads to rapid decreases in δ^2H_R . For instance, in the extreme precipitation process of June 2011, the



501 $\delta^2\text{H}_R$ was reduced by -15.7% under a precipitation input of 144.7 mm from June 5 to
502 June 16, while the $\delta^2\text{H}_R$ decreased by -27.5% with a precipitation input of 487.1 mm
503 in the extreme precipitation process from June 21 to July 1, 2017. Subsequently, in the
504 summer drought periods of 2011 and 2017, the river water isotope gradually enriched
505 to approximately -38% (Fig. 10e and 10f).

506 **5. Discussion**

507 **5.1 Factors that influence the seasonality in river water isotopes**

508 The river water isotopes showed strong seasonality and were influenced by
509 various factors such as precipitation input and evaporation. For instance, in the major
510 flood period and summer drought period, the $\delta^2\text{H}_R$ usually reflected isotope-depleted
511 precipitation inputs, indicating the “amount effect” by the precipitation input.
512 Specifically, the precipitation isotopes were relatively depleted in these two periods,
513 while the river water isotopes captured the precipitation input signal particularly when
514 the 5-day accumulated precipitation exceeded 19.0 mm (i.e. the threshold
515 precipitation amount) (Fig. 5). Additionally, the extreme precipitation events mainly
516 occurred in the major flood period, resulting in relatively isotope-depleted
517 precipitation that was reflected as negative records in the $\delta^2\text{H}_R$ (Fig. 2 and 10). In the
518 summer drought period, the river water isotopes exhibited a gradual enrichment
519 process due to the influence of evaporation and limited precipitation input (Fig. 2 and
520 9). In the rainless period, the $\delta^2\text{H}_R$ values were more positive compared to the summer
521 drought period (Fig. 3b), possibly influenced by precipitation input, evaporation
522 enrichment, and groundwater recharge. Furthermore, the $\delta^2\text{H}_R$ reached the highest
523 positive values in the spring flood period, influenced by relatively isotope-enriched
524 precipitation inputs as mentioned above (Fig. 2 and 3).

525 By examining the relationship between the $\Delta\delta^2\text{H}_R$ and the corresponding



526 accumulated evaporation, it becomes evident that a stronger correlation between the
527 two variables emerges at time intervals exceeding 10 days (Fig. 6). This suggests that
528 the influence of evaporation on river water isotopes manifests over relatively long
529 time intervals, spanning from tens of days to even several months, particularly in long
530 dry periods without precipitation input (Fig. 9). The influences of evaporation on river
531 water isotopes occurs gradually, making it challenging to capture using short-term
532 analyses. Conversely, as indicated by Xiao et al. (2022a), the relatively weak
533 influence of evaporation on river water isotopes observed at short intervals (Fig. 6 and
534 7) can be attributed to the significant influx of precipitation input (i.e. new water)
535 rapidly flowing into the river network, which experiences limited evaporation effects
536 in the relatively short residence time. Furthermore, the variation in runoff discharge
537 exhibits a notable relationship with the $\Delta\delta^2\text{H}_R$ (Fig. 8), however, it is important to note
538 that the decline in runoff discharge may not be solely due to evaporation but could
539 also be influenced by water transport from the Xiangjiang River to the Dongting Lake
540 due to rapid downstream drainage (Zhan et al., 2015), this introduces uncertainties in
541 the analysis based on the changes of runoff discharge and river water isotopes
542 between different time intervals.

543 River water isotopes serve as a valuable record not only for detecting the isotopic
544 depletion signal of extreme precipitation input in the major flood period (Fig. 10) but
545 also for capturing the influence of moderate precipitation in the summer drought
546 period. In the latter case, the river water isotopes gradually become enriched with the
547 decrease of the runoff discharge in prolonged periods of drought. When the basin is
548 relatively dry—that is, the reserves of soil water, groundwater, and river water are
549 limited, the river water may be influenced by a medium precipitation amount,
550 resulting in a highly depleted river water isotope signal observed in this extended river



551 water sample series. For instance, following a precipitation input of 53.5 mm with a
552 $\delta^2\text{H}_\text{P}$ of -68.1‰ on August 23, 2013 (Fig. 9c), the river water isotopes exhibited a
553 significant depletion (Fig. 9e). Notably, the $\delta^2\text{H}_\text{R}$ rapidly declined from -35.7‰ on
554 August 21 to -63.7‰ on September 1, representing the most negative $\delta^2\text{H}_\text{R}$ value
555 observed over the 13-year observations. This $\delta^2\text{H}_\text{R}$ signal differs significantly from
556 rapid decreases in $\delta^2\text{H}_\text{R}$ caused by extreme precipitation input in the river water (Fig.
557 10), highlighting the importance of careful consideration when reconstructing
558 precipitation based on isotopic signals derived from river water. Overall, the
559 seasonality of river water isotopes in the Xiangjiang River basin is influenced by
560 various complex factors, including precipitation input, seasonal drought, and the basin
561 wetness conditions, such as soil water, groundwater, and river water reserves within
562 the channel system.

563 **5.2 Environmental significance implied by the seasonality of river** 564 **water isotopes**

565 The Xiangjiang River, serving as a significant inflow water source, exerts
566 influence on the hydrologic and isotope mass balance of Dongting Lake, the
567 second-largest freshwater lake in China (Zhan et al., 2015; Zhou et al., 2019). The
568 isotopic composition of lake water primarily reflects the input waters, including lake
569 surface precipitation and inflowing river water (Steinman and Abbott, 2013; Gibson et
570 al., 2016; Xiao et al., 2022b), while the isotopic information in lake water can also
571 influence the stable isotopic signatures preserved in lake sediment. Consequently,
572 proxy indicators recorded in lake sediments can be utilized for paleoclimate
573 reconstruction, benefiting from the relationships between the input water isotopes and
574 the local environments.

575 Through the analysis of river water isotopes and various hydrometeorological



576 factors on a seasonal scale, it becomes evident that the $\Delta\delta^2\text{H}_R$ can reflect the
577 corresponding accumulated evaporation and precipitation input (Fig. 5, 6, and 7) and
578 the decline in runoff discharge (Fig. 8) at the observed time intervals. Moreover, river
579 water isotopes entering the lakes can record signals of extreme precipitation (Fig. 10)
580 or exhibit gradual isotopic enrichment under the influence of evaporation in relatively
581 dry periods spanning tens of days or even several months without precipitation (Fig.
582 9). Besides, the isotopic characteristics of precipitation are governed by large-scale
583 factors such as moisture sources, upstream effects, and circulation patterns, and are
584 less influenced by local meteorological factors (Aggarwal et al., 2016; Zhou et al.,
585 2019), thus the river water isotopes are better suited to reflect local environments.
586 Consequently, in comparison to the isotopic characteristics of precipitation, the river
587 water isotopes may provide valuable insights into the relationship between the proxy
588 indicators and the local environments.

589 In previous studies, due to limited data availability, the inflow water isotopes of
590 the lake were often represented by the volume-weighted precipitation isotopes in
591 hydrologic and isotope mass-balance models (e.g., Steinman and Abbott, 2013;
592 Skrzypek et al., 2015; Jones et al., 2016). However, based on the 13-year observations
593 conducted in this study, the annual volume-weighted $\delta^2\text{H}_R$ and $\delta^2\text{H}_P$ were found to
594 closely match only in the period of 2012-2015, with differences within 2‰ (Table 2).
595 In other years, the annual volume-weighted $\delta^2\text{H}_P$ was either more negative or more
596 positive compared to the annual volume-weighted $\delta^2\text{H}_R$. These differences in the
597 annual $\delta^2\text{H}_R$ and $\delta^2\text{H}_P$ were mainly influenced by the seasonality of $\delta^2\text{H}_P$ and
598 precipitation amount. For instance, significant variations were observed between the
599 volume-weighted $\delta^2\text{H}_P$ and $\delta^2\text{H}_R$ in the different runoff periods (Table 2). Therefore,
600 representing the inflow water of the lake solely by the annual volume-weighted



601 precipitation isotopes can only serve as a rough estimation. To accurately depict the
 602 detailed variations in the lake hydrologic and isotope mass balance, more
 603 comprehensive observations of the inflowing river water are required.

604 Table 2. Annual volume-weighted precipitation $\delta^2\text{H}$ and river water $\delta^2\text{H}$ ($\delta^2\text{H}_\text{R}$
 605 and $\delta^2\text{H}_\text{P}$) and volume-weighted average values in different runoff periods. The letters
 606 (RL, SF, MF, and SD) represent the rainless period, spring flood period, major flood
 607 period, and summer drought period, respectively.

| Year | Annual $\delta^2\text{H}_\text{R}$ | Annual $\delta^2\text{H}_\text{P}$ | $\delta^2\text{H}_\text{R}$ in RL | $\delta^2\text{H}_\text{P}$ in RL | $\delta^2\text{H}_\text{R}$ in SF | $\delta^2\text{H}_\text{P}$ in SF | $\delta^2\text{H}_\text{R}$ in MF | $\delta^2\text{H}_\text{P}$ in MF | $\delta^2\text{H}_\text{R}$ in SD | $\delta^2\text{H}_\text{P}$ in SD |
|------|------------------------------------|------------------------------------|-----------------------------------|-----------------------------------|-----------------------------------|-----------------------------------|-----------------------------------|-----------------------------------|-----------------------------------|-----------------------------------|
| 2010 | -34.6 | -48.0 | -38.1 | -54.6 | -26.7 | -16.8 | -36.0 | -47.8 | -40.1 | -73.6 |
| 2011 | -36.9 | -45.3 | -37.4 | -52.0 | -30.3 | -11.4 | -39.0 | -54.3 | -38.9 | -49.3 |
| 2012 | -36.3 | -38.2 | -36.9 | -29.8 | -31.1 | -15.4 | -37.9 | -50.9 | -45.9 | -47.0 |
| 2013 | -33.9 | -33.3 | -35.6 | -72.1 | -27.1 | -3.7 | -30.2 | -28.3 | -48.0 | -47.7 |
| 2014 | -29.0 | -27.7 | -33.2 | -27.3 | -26.3 | -10.8 | -27.8 | -34.5 | -36.0 | -57.1 |
| 2015 | -34.4 | -36.1 | -38.4 | -43.9 | -27.3 | -10.6 | -30.1 | -34.4 | -40.6 | -64.0 |
| 2016 | -31.4 | -40.0 | -35.5 | -31.6 | -27.8 | -16.2 | -30.2 | -50.3 | -36.2 | -67.7 |
| 2017 | -36.4 | -48.2 | -35.0 | -26.6 | -27.4 | -14.5 | -41.2 | -59.3 | -39.4 | -75.4 |
| 2018 | -34.7 | -39.1 | -35.8 | -30.0 | -30.6 | -8.1 | -33.2 | -49.5 | -39.5 | -67.6 |
| 2019 | -31.8 | -24.0 | -30.8 | -25.3 | -26.4 | -2.5 | -34.2 | -31.2 | -36.4 | -28.7 |
| 2020 | -28.5 | -36.9 | -32.2 | -31.3 | -24.2 | -9.2 | -28.4 | -43.2 | -28.0 | -54.6 |
| 2021 | -30.1 | -32.4 | -36.3 | -31.1 | -28.3 | -12.1 | -28.2 | -32.4 | -32.6 | -66.5 |
| 2022 | -36.1 | -39.2 | -34.2 | -47.8 | -32.1 | -18.1 | -37.5 | -46.6 | -42.8 | -50.2 |

608 Nevertheless, according to the analysis on an annual scale based on the 13-year
 609 observations, the volume-weighted $\delta^2\text{H}_\text{R}$ values in the different runoff periods did not
 610 exhibit significant correlations with the corresponding total precipitation, average
 611 runoff discharge, average air temperature, and total evaporation (Fig. S4). Although
 612 this study encompasses 13-year observations with a sampling interval of five days,
 613 there is a need for longer and systematic observations of various water types and
 614 hydrometeorological factors, spanning decadal or longer time scales, to better
 615 elucidate the relationships between river water isotopes and local environments on the
 616 annual scale.

617 **5.3 The representation of the Changsha site in the Xiangjiang River**



618 **basin**

619 The increases in runoff discharge and water level in the Changsha section of the
620 Xiangjiang River are primarily attributed to the precipitation recharge in the middle
621 and upper reaches, while the influences of evaporation on river water isotopes mainly
622 occur within the basin. It should be noted that the sampling and observation sites for
623 precipitation, air temperature, and evaporation in this study, located at Hunan Normal
624 University and National Meteorological Reference Station in Changsha, respectively,
625 only represent the local conditions in Changsha. Therefore, the extent of their
626 influence on the runoff discharge and water stable isotopes of the entire Xiangjiang
627 River may be limited. To assess whether the sampling and observations in Changsha
628 can adequately represent the Xiangjiang River basin, a spatial correlation analysis was
629 conducted between the Changsha site and the surrounding regions based on data from
630 1979 to 2021, including precipitation isotopes, precipitation amount, evaporation, and
631 air temperature (Fig. S5). The analysis employed the simulated precipitation isotope
632 data generated by the isotopic Atmospheric Water Balance Model (iAWBM) as
633 detailed by Zhang et al. (2015), which has a spatial resolution of $1.5^{\circ} \times 1.5^{\circ}$, while the
634 air temperature, evaporation, and precipitation amount data from the ERA5 reanalysis
635 dataset (<https://cds.climate.copernicus.eu>) published by the European Centre for
636 Medium-Range Weather Forecasts (ECMWF), which has a spatial resolution of $1^{\circ} \times$
637 1° . Overall, all the data employed in this spatial correlation analysis was integrated
638 into a 5-day interval.

639 The results of spatial correlation analysis revealed a high correlation between the
640 reanalysis data of air temperature and evaporation at the Changsha site and those in
641 the surrounding regions, with correlation coefficients above 0.8 and $p < 0.001$ for the
642 grid points in the Xiangjiang River basin (Fig. S5a and S5b). Furthermore, while the



643 relationship between the reanalysis data of precipitation amount and simulated
644 precipitation isotopes at the Changsha site and in the surrounding regions is not as
645 strong as that for air temperature and evaporation, the correlation is still high (Fig.
646 S5c and S5d). For instance, the correlation coefficients between the Changsha site and
647 the grid points in the Xiangjiang River basin exceed 0.7 with $p < 0.001$ for both the
648 reanalysis data of precipitation amount and simulated precipitation isotopes (Fig. S5c
649 and S5d). Overall, the high correlation coefficients for these factors support the time
650 consistency between the Changsha site and the surrounding regions, while the high
651 spatial consistency is characterized by the large area of the high correlation
652 coefficients, which covers the whole Xiangjiang River basin. These spatial correlation
653 analyses provide support for the representation of hydrometeorological factors and
654 precipitation isotopes at the Changsha site with the Xiangjiang River basin to a certain
655 extent. In addition, the next step involves expanding the observation of air
656 temperature, evaporation, and precipitation amount and the sampling of precipitation
657 samples along the middle and upper reaches of the Xiangjiang River, this will help
658 further validate the representativeness of the observations at the Changsha site for the
659 entire Xiangjiang River basin.

660 **6. Conclusions**

661 The main findings of this study are as follows: (1) Both the $\delta^2\text{H}_\text{P}$ and $\delta^2\text{H}_\text{R}$
662 displayed significant seasonal variation throughout the year, the average $\delta^2\text{H}_\text{R}$ was
663 ranked as follows: spring flood period, major flood period, rainless period, and
664 summer drought period. The temporal pattern of the $\delta^2\text{H}_\text{R}$ was similar but attenuated
665 compared to the $\delta^2\text{H}_\text{P}$, indicating the influences of direct precipitation input,
666 evaporation, and mixing with older waters. (2) The $\delta^2\text{H}_\text{R}$ showed a weak correlation
667 with the corresponding accumulated precipitation amount or average runoff discharge,



668 which can be attributed to the mixing between the new input precipitation and the old
669 waters within the basin. The relationship between the $\delta^2\text{H}_R$ and the corresponding
670 average air temperature or accumulated evaporation may be masked by the
671 precipitation inputs, as the relationship between precipitation isotopes and air
672 temperature exhibits strong seasonality. (3) The ΔR and $\Delta\delta^2\text{H}_R$ exhibited significant
673 responses to the corresponding accumulated precipitation, with heavier precipitation
674 events more likely to alter runoff discharge and river water isotopes. The $\Delta\delta^2\text{H}_R$
675 showed a notably positive correlation with the corresponding accumulated
676 evaporation and average ΔR , particularly at longer time intervals without precipitation
677 input. (4) In the major flood period, the $\delta^2\text{H}_R$ may rapidly decrease with a maximum
678 decrease range of -27.5% due to the input of extreme precipitation with relatively
679 depleted isotopes, while the river water isotopes gradually enriched in the subsequent
680 summer drought period. In the summer drought periods of 2013 and 2022, the runoff
681 discharge and $\delta^2\text{H}_R$ showed gradual decrease and increase, respectively, with the $\delta^2\text{H}_R$
682 potentially increasing by up to 20.2% influenced by the extreme drought.

683 The $\Delta\delta^2\text{H}_R$ at 5-day or longer intervals serves as a variable that was influenced
684 by the hydrometeorological factors, such as the accumulated evaporation and
685 precipitation input and the decline in runoff discharge, thus providing insights into the
686 relationship between the river water isotopes and the seasonality of local
687 environments, making it valuable for paleoclimate reconstruction. The influences of
688 evaporation on river water isotopes occur gradually at relatively long time intervals.
689 However, the spring flood period shows the most positive $\delta^2\text{H}_R$ due to the input of
690 enriched precipitation isotopes. In contrast, in the summer drought period, when basin
691 wetness conditions are limited, the input of moderate precipitation leads to the most
692 negative $\delta^2\text{H}_R$ observed over the 13-year observations. Therefore, caution should be



693 exercised when using isotopic signals of river water to reconstruct local environments
694 such as precipitation, air temperature, evaporation, and runoff discharge. The spatial
695 correlation analysis confirms the association between the precipitation amount,
696 evaporation, air temperature, and precipitation isotopes at the Changsha site with the
697 Xiangjiang River basin. To enhance the reliability of the observations and ensure their
698 representativeness for the entire Xiangjiang River basin, further comprehensive
699 measurements of hydrometeorological factors and sampling of precipitation samples
700 are needed within the basin itself.

701 **Code/Data availability**

702 The data that support the findings of this study are available from the corresponding
703 author upon reasonable request

704 **Author contribution**

705 Xiong Xiao: Data curation, Methodology, Software, Writing – original draft, &
706 editing. Xinping Zhang: Methodology, Writing – original draft, & editing. Zhiguo Rao,
707 Xinguang He, and Cicheng Zhang: Methodology.

708 **Competing interests**

709 The authors declare that they have no known competing financial interests or personal
710 relationships that could have appeared to influence the work reported in this paper.

711 **Acknowledgments**

712 This study was supported by the Natural Science Foundation of Hunan Province,
713 China (No. 2023JJ40445) and the National Natural Science Foundation of China (No.
714 42101130). We are grateful to the graduate students who laboriously sampled water
715 samples without interruption and tested water stable isotopes in the 13 hydrological
716 years.

717 **References:**



- 718 Aggarwal, P. K., Romatschke, U., Araguas-Araguas, L., Belachew, D., Longstaffe, F.
719 J., Berg, P., ... & Funk, A. (2016). Proportions of convective and stratiform
720 precipitation revealed in water isotope ratios. *Nature Geoscience*, 9(8), 624-629.
721 <https://doi.org/10.1038/ngeo2739>
- 722 Allen, R. G., Pereira, L. S., Smith, M., Raes, D., & Wright, J. L. (2005). FAO-56 dual
723 crop coefficient method for estimating evaporation from soil and application
724 extensions. *Journal of Irrigation and Drainage Engineering*, 131(1), 2-13.
725 [https://doi.org/10.1061/\(ASCE\)0733-9437\(2005\)131:1\(2\)](https://doi.org/10.1061/(ASCE)0733-9437(2005)131:1(2))
- 726 Bonaldo, D., Bellafiore, D., Ferrarin, C., Ferretti, R., Ricchi, A., Sangelantoni, L., &
727 Vitelletti, M. L. (2023). The summer 2022 drought: a taste of future climate for
728 the Po valley (Italy). *Regional Environmental Change*, 23(1), 1.
729 <https://doi.org/10.1007/s10113-022-02004-z>
- 730 Boral, S., Sen, I. S., Ghosal, D., Peucker-Ehrenbrink, B., & Hemingway, J. D. (2019).
731 Stable water isotope modeling reveals spatio-temporal variability of glacier
732 meltwater contributions to Ganges River headwaters. *Journal of Hydrology*, 577,
733 123983. <https://doi.org/10.1016/j.jhydrol.2019.123983>
- 734 Boutt, D. F., Mabee, S. B., & Yu, Q. (2019). Multiyear increase in the stable isotopic
735 composition of stream water from groundwater recharge due to extreme
736 precipitation. *Geophysical Research Letters*, 46(10), 5323-5330.
737 <https://doi.org/10.1029/2019GL082828>
- 738 Cardoso Pereira, S., Marta-Almeida, M., Carvalho, A. C., & Rocha, A. (2020).
739 Extreme precipitation events under climate change in the Iberian Peninsula.
740 *International Journal of Climatology*, 40(2), 1255-1278.
741 <https://doi.org/10.1002/joc.6269>



- 742 Cook, B. I., Mankin, J. S., & Anchukaitis, K. J. (2018). Climate change and drought:
743 From past to future. *Current Climate Change Reports*, 4, 164-179.
744 <https://doi.org/10.1007/s40641-018-0093-2>
- 745 Craig, H. (1961). Standard for reporting concentrations of deuterium and oxygen-18
746 in natural waters. *Science*, 133(3467), 1833–1834.
747 <https://doi.org/10.1126/science.133.3465.1702>
- 748 Dansgaard, W. (1964). Stable isotopes in precipitation. *Tellus*, 16(4), 436-468.
749 <https://doi.org/10.3402/tellusa.v16i4.8993>
- 750 Das, S., & Rai, S. K. (2022). Stable isotopic variations (δD and $\delta^{18}O$) in a
751 mountainous river with rapidly changing altitude: Insight into the hydrological
752 processes and rainout in the basin. *Hydrological Processes*, 36(3), e14547.
753 <https://doi.org/10.1002/hyp.14547>
- 754 Emmanouilidis, A., Katrantsiotis, C., Dotsika, E., Kokkalas, S., Unkel, I., &
755 Avramidis, P. (2022). Holocene paleoclimate variability in the eastern
756 Mediterranean, inferred from the multi-proxy record of Lake Vouliagmeni,
757 Greece. *Palaeogeography, Palaeoclimatology, Palaeoecology*, 595, 110964.
758 <https://doi.org/10.1016/j.palaeo.2022.110964>
- 759 Gibson, J. J., Birks, S. J., & Yi, Y. (2016). Stable isotope mass balance of lakes: a
760 contemporary perspective. *Quaternary Science Reviews*, 131, 316-328.
761 <https://doi.org/10.1016/j.quascirev.2015.04.013>
- 762 Grillakis, M. G. (2019). Increase in severe and extreme soil moisture droughts for
763 Europe under climate change. *Science of the Total Environment*, 660, 1245-1255.
764 <https://doi.org/10.1016/j.scitotenv.2019.01.001>
- 765 Hua, M., Zhang, X., Yao, T., Luo, Z., Zhou, H., Rao, Z., & He, X. (2019). Dual effects
766 of precipitation and evaporation on lake water stable isotope composition in the



- 767 monsoon region. *Hydrological Processes*, 33(16), 2192-2205.
768 <https://doi.org/10.1002/hyp.13462>
- 769 Huang, R., Xu, L., Yuan, X., Lu, R., Sung-Eui, M., & Ung-Jun, K. (1998). Seasonal
770 prediction experiments of the summer droughts and floods during the early
771 1990's in East Asia with numerical models. *Advances in Atmospheric Sciences*,
772 15, 433-446. <https://doi.org/10.1007/s00376-998-0025-5>
- 773 Jiang, D., Li, Z., Luo, Y., & Xia, Y. (2021). River damming and drought affect water
774 cycle dynamics in an ephemeral river based on stable isotopes: The Dagu River
775 of North China. *Science of the Total Environment*, 758, 143682.
776 <https://doi.org/10.1016/j.scitotenv.2020.143682>
- 777 Jiménez-Iñiguez, A., Ampuero, A., Valencia, B. G., Mayta, V. C., Cruz, F. W., Vuille,
778 M., ... & Conicelli, B. (2022). Stable isotope variability of precipitation and cave
779 drip-water at Jumandy cave, western Amazon River basin (Ecuador). *Journal of*
780 *Hydrology*, 610, 127848. <https://doi.org/10.1016/j.jhydrol.2022.127848>
- 781 Jones, M. D., Cuthbert, M. O., Leng, M. J., McGowan, S., Mariethoz, G., Arrowsmith,
782 C., ... & Cross, I. (2016). Comparisons of observed and modelled lake $\delta^{18}\text{O}$
783 variability. *Quaternary Science Reviews*, 131, 329-340.
784 <https://doi.org/10.1016/j.quascirev.2015.09.012>
- 785 Ma, M., Qu, Y., Lyu, J., Zhang, X., Su, Z., Gao, H., ... & Wang, Z. (2022). The 2022
786 extreme drought in the Yangtze River Basin: Characteristics, causes and response
787 strategies. *River*, 1(2), 162-171. <https://doi.org/10.1002/rvr2.23>
- 788 Marengo, J. A., Alves, L. M., Ambrizzi, T., Young, A., Barreto, N. J., & Ramos, A. M.
789 (2020). Trends in extreme rainfall and hydrogeometeorological disasters in the
790 Metropolitan Area of São Paulo: a review. *Annals of the New York Academy of*
791 *Sciences*, 1472(1), 5-20. <https://doi.org/10.1111/nyas.14307>



- 792 Muñoz-Villers, L. E., & McDonnell, J. J. (2013). Land use change effects on runoff
793 generation in a humid tropical montane cloud forest region. *Hydrology and Earth*
794 *System Sciences*, 17(9), 3543-3560. <https://doi.org/10.5194/hess-17-3543-2013>
- 795 Nkemelang, T., New, M., & Zaroug, M. (2018). Temperature and precipitation
796 extremes under current, 1.5 C and 2.0 C global warming above pre-industrial
797 levels over Botswana, and implications for climate change vulnerability.
798 *Environmental Research Letters*, 13(6), 065016.
799 <https://doi.org/10.1088/1748-9326/aac2f8>
- 800 Qin, S. H, et al. (2006). *Hydrogeology of Hunan Province (in Chinese)*. Hunan
801 hydrology and water resources Survey Bureau. Beijing: China Water & Power
802 Press, pp. 42-50. ISBN: 9787508440637.
- 803 Ren, W., Tian, L., & Shao, L. (2023). Temperature and precipitation control the
804 seasonal patterns of discharge and water isotopic signals of the Nyang River on
805 the southeastern Tibetan Plateau. *Journal of Hydrology*, 617, 129064.
806 <https://doi.org/10.1016/j.jhydrol.2023.129064>
- 807 Rode, M., Wade, A. J., Cohen, M. J., Hensley, R. T., Bowes, M. J., Kirchner, J. W., ...
808 & Jomaa, S. (2016). Sensors in the stream: the high-frequency wave of the
809 present. *Sci. Technol.* 50, 10297–10307. <https://doi.org/10.1021/acs.est.6b02155>
- 810 Saranya, P., Krishnakumar, A., Kumar, S., & Krishnan, K. A. (2020). Isotopic study
811 on the effect of reservoirs and drought on water cycle dynamics in the tropical
812 Periyar basin draining the slopes of Western Ghats. *Journal of Hydrology*, 581,
813 124421. <https://doi.org/10.1016/j.jhydrol.2019.124421>
- 814 Scholl, M., Shanley, J., Murphy, S., Willenbring, J., Occhi, M., & González, G. (2015).
815 Stable-isotope and solute-chemistry approaches to flow characterization in a



816 forested tropical watershed, Luquillo Mountains, Puerto Rico. *Applied*
817 *Geochemistry*, 63, 484–497. <https://doi.org/10.1016/j.apgeochem.2015.03.008>

818 Shi, X., Zhang, F., Tian, L., Joswiak, D. R., Zeng, C., & Qu, D. (2014). Tracing
819 contributions to hydro-isotopic differences between two adjacent lakes in the
820 southern Tibetan Plateau. *Hydrological Processes*, 28(22), 5503-5512.
821 <https://doi.org/10.1002/hyp.10051>

822 Sinha, N., & Chakraborty, S. (2020). Isotopic interaction and source moisture control
823 on the isotopic composition of rainfall over the Bay of Bengal. *Atmospheric*
824 *Research*, 235, 104760. <https://doi.org/10.1016/j.atmosres.2019.104760>

825 Skrzypek, G., Mydłowski, A., Dogramaci, S., Hedley, P., Gibson, J. J., & Grierson, P.
826 F. (2015). Estimation of evaporative loss based on the stable isotope composition
827 of water using Hydrocalculator. *Journal of Hydrology*, 523, 781-789.
828 <https://doi.org/10.1016/j.jhydrol.2015.02.010>

829 Sprenger, M., Llorens, P., Gallart, F., Benettin, P., Allen, S. T., & Latron, J. (2022).
830 Precipitation fate and transport in a Mediterranean catchment through models
831 calibrated on plant and stream water isotope data. *Hydrology and Earth System*
832 *Sciences*, 26(15), 4093-4107. <https://doi.org/10.5194/hess-26-4093-2022>

833 Steinman, B. A., & Abbott, M. B. (2013). Isotopic and hydrologic responses of small,
834 closed lakes to climate variability: Hydroclimate reconstructions from lake
835 sediment oxygen isotope records and mass balance models. *Geochimica et*
836 *Cosmochimica Acta*, 105, 342-359. <https://doi.org/10.1016/j.gca.2012.11.027>

837 Steinman, B. A., Rosenmeier, M. F., Abbott, M. B., & Bain, D. J. (2010). The isotopic
838 and hydrologic response of small, closed-basin lakes to climate forcing from
839 predictive models: Application to paleoclimate studies in the upper Columbia



- 840 River basin. *Limnology and Oceanography*, 55(6), 2231-2245.
841 <https://doi.org/10.4319/lo.2010.55.6.2231>
- 842 Streletskiy, D. A., Tananaev, N. I., Opel, T., Shiklomanov, N. I., Nyland, K. E.,
843 Streletskaya, I. D., & Shiklomanov, A. I. (2015). Permafrost hydrology in
844 changing climatic conditions: seasonal variability of stable isotope composition
845 in rivers in discontinuous permafrost. *Environmental Research Letters*, 10(9),
846 095003. <https://doi.org/10.1088/1748-9326/10/9/095003>
- 847 Sun, Z., Zhu, G., Zhang, Z., Xu, Y., Yong, L., Wan, Q., ... & Liu, Y. (2021). Identifying
848 surface water evaporation loss of inland river basin based on evaporation
849 enrichment model. *Hydrological Processes*, 35(3), e14093.
850 <https://doi.org/10.1002/hyp.14093>
- 851 Uchiyama, R., Okochi, H., Ogata, H., Katsumi, N., Asai, D., & Nakano, T. (2017). H
852 and O isotopic differences in typhon and urban-induced heavy rain in Tokyo.
853 *Environmental Chemistry Letters*, 15, 739-745.
854 <https://doi.org/10.1007/s10311-017-0652-0>
- 855 von Freyberg, J., R ücker, A., Zappa, M., Schlumpf, A., Studer, B., & Kirchner, J. W.
856 (2022). Four years of daily stable water isotope data in stream water and
857 precipitation from three Swiss catchments. *Scientific data*, 9(1), 46.
858 <https://doi.org/10.1038/s41597-022-01148-1>
- 859 von Freyberg, J., Studer, B., & Kirchner, J. W. (2017). A lab in the field:
860 high-frequency analysis of water quality and stable isotopes in stream water and
861 precipitation. *Hydrology and Earth System Sciences*, 21(3), 1721-1739.
862 <https://doi.org/10.5194/hess-21-1721-2017>
- 863 Wang, L., Dong, Y., Xie, Y., & Chen, M. (2023). Hydrological processes and water
864 quality in arid regions of Central Asia: insights from stable isotopes and



- 865 hydrochemistry of precipitation, river water, and groundwater. *Hydrogeology*
866 *Journal*, 1-17. <https://doi.org/10.1007/s10040-023-02654-1>
- 867 Wang, Q., Huang, G., Wang, L., Piao, J., Ma, T., Hu, P., ... & Limsakul, A. (2023).
868 Mechanism of the summer rainfall variation in Transitional Climate Zone in East
869 Asia from the perspective of moisture supply during 1979–2010 based on the
870 Lagrangian method. *Climate Dynamics*, 60(3-4), 1225-1238.
871 <https://doi.org/10.1007/s00382-022-06344-8>
- 872 Wu, H., Huang, Q., Fu, C., Song, F., Liu, J., & Li, J. (2021). Stable isotope signatures
873 of river and lake water from Poyang Lake, China: Implications for river–lake
874 interactions. *Journal of Hydrology*, 592, 125619.
875 <https://doi.org/10.1016/j.jhydrol.2020.125619>
- 876 Xiao, X., Zhang, X., Wu, H., Zhang, C., & Han, L. (2022a). Stable isotopes of surface
877 water and groundwater in a typical subtropical basin in south-central China:
878 Insights into the young water fraction and its seasonal origin. *Hydrological*
879 *Processes*, 36(4), e14574. <https://doi.org/10.1002/hyp.14574>
- 880 Xiao, X., Zhang, C., He, X., & Zhang, X. (2022b). Simulating the water $\delta^{18}\text{O}$ of a
881 small open lake in the East Asian monsoon region based on hydrologic and
882 isotope mass-balance models. *Journal of Hydrology*, 612, 128223.
883 <https://doi.org/10.1016/j.jhydrol.2022.128223>
- 884 Xiao, Z., Zhang, X., Xiao, X., Chang, X., He, X., & Zhang, C. (2023). Comparisons
885 of precipitation isotopic effects on daily, monthly and annual time scales—a case
886 study in the subtropical monsoon region of eastern China. *Water*, 15(3), 438.
887 <https://doi.org/10.3390/w15030438>
- 888 Yang, J., Dudley, B. D., Montgomery, K., & Hodgetts, W. (2020). Characterizing
889 spatial and temporal variation in ^{18}O and ^2H content of New Zealand river water



- 890 for better understanding of hydrologic processes. *Hydrological Processes*, 34(26),
891 5474-5488. <https://doi.org/10.1002/hyp.13962>
- 892 Yao, T., Zhang, X., Li, G., Huang, H., Wu, H., Huang, Y., & Zhang, W. (2016).
893 Characteristics of the stable isotopes in different water bodies and their
894 relationships in surrounding areas of Yuelu Mountain in the Xiangjiang River
895 basin (in Chinese). *Journal of Natural Resources*, 31(7), 1198.
896 <https://doi.org/10.11849/zrzyxb.20150810>
- 897 Zhan, L., Chen, J., Zhang, S., Huang, D., & Li, L. (2015). Relationship between
898 Dongting Lake and surrounding rivers under the operation of the Three Gorges
899 Reservoir, China. *Isotopes in Environmental and Health Studies*, 51(2), 255-270.
900 <https://doi.org/10.1080/10256016.2015.1020306>
- 901 Zhang, X. P., Guan, H. D., Zhang, X. Z., Wu, H. W., Li, G., & Huang, Y. M. (2015).
902 Simulation of stable water isotopic composition in the atmosphere using an
903 isotopic Atmospheric Water Balance Model. *International Journal of Climatology*,
904 35(6), 846-859. <https://doi.org/10.1002/joc.4019>
- 905 Zhi ña, D. X., Mosquera, G. M., Esquivel-Hernández, G., Córdova, M.,
906 Sánchez-Murillo, R., Orellana-Alvear, J., & Crespo, P. (2022).
907 Hydrometeorological factors controlling the stable isotopic composition of
908 precipitation in the highlands of south Ecuador. *Journal of Hydrometeorology*,
909 23(7), 1059-1074. <https://doi.org/10.1175/JHM-D-21-0180.1>
- 910 Zhou, H., Zhang, X., Yao, T., Hua, M., Wang, X., Rao, Z., & He, X. (2019). Variation
911 of $\delta^{18}\text{O}$ in precipitation and its response to upstream atmospheric convection and
912 rainout: A case study of Changsha station, south-central China. *Science of the*
913 *Total Environment*, 659, 1199-1208.
914 <https://doi.org/10.1016/j.scitotenv.2018.12.396>



915 Zhou, J., Wan, R. R., Li, B., & Dai, X. (2019). Assessing the impact of climate change
916 and human activities on runoff in the Dongting Lake basin of China. Applied
917 Ecology & Environmental Research, 17(3).
918 http://dx.doi.org/10.15666/aeer/1703_57975812